7-2014

Application of the Savitzky-Golay Filter to Land Cover Classification Using Temporal MODIS Vegetation Indices

So-Ra Kim
Korea University

Anup K. Prasad
Chapman University

Hesham el-Askary
Chapman University, elaskary@chapman.edu

Woo- Kyun Lee
Korea University

Doo- Ahn Kwak
Korea University

See next page for additional authors

Application of the Savitzky-Golay Filter to Land Cover Classification Using Temporal MODIS Vegetation Indices

Authors

So-Ra Kim, Anup K. Prasad, Hesham el-Askary, Woo- Kyun Lee, Doo- Ahn Kwak, Seung- Ho Lee, and Menas Kafatos

Application of the Savitzky-Golay Filter to Land Cover Classification Using Temporal MODIS Vegetation Indices

So-Ra Kim, Anup K. Prasad, Hesham El-Askary, Woo-Kyun Lee, Doo-Ahn Kwak, Seung-Ho Lee, and Menas Kafatos

Abstract

In this study, the Savitzky-Golay filter was applied to smooth observed unnatural variations in the temporal profiles of the Normalized Difference Vegetation Index (NDVI) and the Enhanced Vegetation Index (EVI) time series from the MODerate Resolution Imaging Spectroradiometer (MODIS). We computed two sets of land cover classifications based on the NDVI and EVI time series before and after applying the Savitzky-Golay filter. The resulting classification from the filtered versions of the vegetation indices showed a substantial improvement in accuracy when compared to the classifications from the unfiltered versions. The classification by the EVIsg had the highest $\hat{K}$ (0.72) for all classes compared to those of the EVI (0.67), NDVI (0.63), and NDVIsg (0.62). Therefore, we conclude that the EVIsg is best suited for land cover classification compared to the other data sets in this study.

Introduction

Land cover data provide key environmental information for many scientific and policy applications, including resource management. They play a pivotal role in evaluating ecosystem processes and human activities (Cihlar, 2000; Homer *et al.*, 2004; Marland *et al.*, 2003). Remote sensing has recently become an important tool for preparing land use maps to support a wide range of environmental research and planning activities. Moreover, classification of spectral images has become

So-Ra Kim and Woo-Kyun Lee are with Korea University, Division of Environmental Science and Ecological Engineering, Korea University, Seoul 136-713, Republic of Korea (leewk@ Korea.ac.kr).

Anup K. Prasad and Menas Kafatos are with Chapman University, School of Earth and Environmental Sciences, Schmid College of Science, Chapman University, Orange, CA 92866, and Center of Excellence in Earth Observing, Chapman University, Orange, CA, 92866.

Hesham El-Askary is with Chapman University, Alexandria University, School of Earth and Environmental Sciences, Schmid College of Science, Chapman University, Orange CA 92866; Center of Excellence in Earth Observing, Chapman University, Orange, CA, 92866; and Department of Environmental Sciences, Faculty of Science, Alexandria University, Moharem Bek, Alexandria, 21522, Egypt.

Doo-Ahn Kwak is with Korea University, GIS-RS Center for Environmental Resources, Korea University, Seoul 136-713, Republic of Korea.

Seung-Ho Lee is with Korea Forest Research Institute, Division of Forest Economics & Management, Korea Forest Research Institute, Seoul, 130-712, Republic of Korea.

a particularly useful application for deriving land cover maps (Heinl *et al.*, 2009; Herold *et al.*, 2008; Xia *et al.*, 2008). Conventional procedures for land cover assessment generally use one or more image sources such as those obtained from Landsat, the Advanced Spaceborne Thermal Emission and Reflection Radiometer (ASTER), the Advanced Very High Resolution Radiometer (AVHRR), and other remotely sensed data (Bakr *et al.*, 2010; Samaniego and Schulz, 2009). However, such remotely sensed data have some limitations such as spatial and temporal resolutions, availability of data, and overall cost considerations (Lunetta *et al.*, 2006; Wardlow *et al.*, 2007).

The MODerate Resolution Imaging Spectroradiometer (MODIS) onboard the Terra and Aqua satellites, offers an opportunity for large-scale land cover characterization. MODIS provides high-quality regional as well as global coverage with high temporal (daily, 8-day, 16-day, and monthly composites) and intermediate spatial (250 m) resolution (Justice and Townshend, 2002; Knight and Lunetta, 2006; Lunetta *et al.*, 2006). Wessels *et al.* (2004) found that typical land cover classes such as agriculture regions, deciduous/evergreen forests, and grassland areas could be successfully mapped using MODIS 250 m data. Dash *et al.* (2007) used two operational Medium Resolution Imaging Spectrometer (MERIS)-derived vegetation indices (at 300 m spatial resolution), forming the MERIS global vegetation index (MGVI) and the MERIS terrestrial chlorophyll index (MTCI), for land cover classification and mapping, and achieved good accuracy (73.2 percent). They also found a high degree of inter-class separability that varied seasonally, resulting in higher accuracy in certain periods. Knight and Lunetta (2003) suggested that the minimum mapping unit should be close to the native resolution of the sensor, since the resampling process to create coarser resolution data also increases the associated errors.

Moreover, time-series signatures derived from repeated sampling of the study area throughout the year based on satellite observations are increasingly being used by agricultural scientists, ecologists, and environmentalists (Friedl *et al.*, 2002; Doraiswamy *et al.*, 2005; Knight and Lunetta, 2006; Oliveira *et al.*, 2010; Sulla-Menashe *et al.*, 2011). In some cases, the temporal signature proved to be more important than spectral information from multiple bands or image texture for identification of specific forest types, such as semi-deciduous Atlantic forest (Carvalho *et al.*, 2004). National Oceanic and Atmospheric Administration (NOAA)/AVHRR time-series data

(1.1 km resolution) have been used by Fischer (1994) in a semi-empirical model to identify unique inflexion points in the phenological signature that provide useful information on actual crop development. NOAA/AVHRR-derived Normalized Difference Vegetation Index (NDVI) temporal profiles (time-series signatures) have been used to monitor the phenological stages for soybean yield forecasting, and to track the biomass of this crop (Esquerdo et al., 2011). The spatial distribution of phenological metrics estimated from MODIS data is qualitatively realistic, and exhibits strong correspondence with temperature patterns in mid- and high-latitude climates, with rainfall seasonality in seasonally dry climates, and with cropping patterns in agricultural area (Zhang et al., 2006).

The VI was developed on the basis of the unique spectral characteristics of green vegetation in the visible and near-infrared wavelengths (Verstraete and Pinty, 1996). Although there are several methods for calculating VI using these two spectral bands, the NDVI has been the most widely used in applied remote sensing. The NDVI is calculated by dividing the difference between the two spectral reflectance values by their sum (Tucker et al., 1991). Furthermore, the EVI is introduced as a modified NDVI that is more resistant to the influence of atmospheric aerosols than NDVI. This is achieved through correction of the red channel using the more aerosol-sensitive blue band (Huete et al., 2002). As such, EVI has improved sensitivity in high biomass regions, and hence, allows for better vegetation monitoring through decoupling of the canopy background signal, and the reduction of atmospheric influences (Huete et al., 2002).Therefore, the EVI is a more suitable measure of greenness of vegetation than NDVI, particularly over regions with relatively high aerosol loading or strong seasonal variations in aerosols.

The potential usage of time-series signatures derived from MODIS-derived vegetation indices such as NDVI and the Enhanced Vegetation Index (EVI) has been identified and emphasized in several studies (Doraiswamy et al., 2005; Galford et al., 2008; Lunetta et al., 2006; Zhang et al., 2003). Lunetta et al. (2006) utilized MODIS NDVI (16-day) time-series data, reducing noise with a discrete Fourier transform technique, for land cover change detection over the Albemarle-Pamlico Estuary System region of the USA. They achieved reasonable accuracy (88 percent with Kappa coefficient of 0.67). Hence, the MODIS time-series data were found to be more useful due to increased temporal resolution even though they have lower spatial resolution compared to Landsat. MODIS vegetation-related parameters and phenology have been used to assess crop biophysical parameters useful to crop yield (corn and soybean) and crop classification (Doraiswamy et al., 2005). The MODIS NDVI data have also been found to be sensitive to an appropriate dynamic range for assessing multi-temporal (seasonal) and spatial vegetation variability (Oliveira et al., 2010). Moreover, Galford et al. (2008) applied wavelet-smoothed time-series on MODIS EVI data to detect expansion of agriculture in Brazil.

It is noteworthy that phenological signatures of time-series data acquired from spaceborne sensors are useful for studying vegetation characteristics (de Jong et al., 2011; Lunetta et al., 2006; Roerink et al., 2000). Roerink et al. (2000) applied the Harmonic Analysis of Time Series (HANTS) algorithm to recognize cloud-affected data for reconstructing gapless AVHRR 10-day maximum NDVI composites over Europe. de Jong et al. (2011) using global NDVI time-series data (1981 to 2006) carried out harmonic analysis with the HANTS algorithm and non-parametric trend analysis to study monotonic greening and browning trends, taking into account phenological shifts and variations in the length of the growing season. On the other hand, Oliveira et al. (2010) applied the HANTS algorithm to smooth and de-noise MODIS vegetation time series. Hird and McDermid (2009) analyzed six methods (Twice filter,

ARMD3-ARMA5 filter; asymmetric Gaussin function-fitting, double logistic function-fitting, MVI filter, and Savitzky-Golay (SG) filter) and concluded that the strength and nature of the noise should be considered when selecting a suitable method for correcting time-series data.

In many studies of vegetation remote sensing, the vegetation index (VI) has been used as a primary measure related to biophysical characteristics of the canopy, such as biomass, productivity, leaf area index (LAI) (Myneni et al., 2002; Zheng and Moskal, 2009; Jia et al., 2009), photosynthetically active radiation (PAR) (Wu et al., 2010; Xiao et al., 2010), and canopy closure (Xu et al., 2003).

Time-series data for the VI derived from TERRA or AQUA (MODIS), NOAA (AVHRR), or SPOT (VEGETATION) have proven to be appropriate for monitoring long-term land use and land cover changes, extracting biophysical and phenological information on the canopy, and modeling terrestrial ecosystems at global, continental, and regional scales (Gu et al., 2009; Wardlow et al., 2007). However, VI time-series data are spatiotemporally discontinuous due to cloud cover, seasonal snow, and atmospheric variability (Chen et al., 2004; Xiao et al., 2003; Xiao et al., 2011). Therefore a number of methods have been developed in recent years to reduce this noise and construct high-quality VI time-series data sets for further analysis (Hird and McDermid, 2009). Reduction of noise in NDVI data, while maintaining the integrity of the NDVI signal, is fundamental to the extraction of phenological information as well as for classification accuracy (Hird and McDermid, 2009). These methods are generally grouped into two types: (a) noise reduction in the frequency domain, such as Fourier-based fitting methods (Roerink et al., 2000; Verhoef et al., 1996), and (b) noise reduction in the temporal domain, based on the best index slope extraction (BISE) algorithm (Viovy et al., 1992), weighed least-squares linear regression (Swets et al., 1999), or asymmetric Gaussian function fitting (Jonsson and Eklundh, 2002). While these methods are commonly used to restore VI multi-temporal profiles, they also suffer from several drawbacks (Jonsson and Eklundh, 2002). Fourier-based fitting methods may generate spurious oscillations when applied to asymmetric NDVI time series, since they depend strongly on symmetric sine and cosine functions (Chen et al., 2004; Roerink et al., 2000). The BISE algorithm requires determination of a sliding period, as well as a threshold for an acceptable percentage increase in NDVI for regrowth during a sliding period, based on an empirical strategy that is generally subjective and depends on the skills and experience of the analyst (Chen et al., 2004; Lovell and Graetz, 2001; Viovy et al., 1992). The asymmetric Gaussian function-fitting approach is more flexible and effective in obtaining a high-quality NDVI time series. However, it may fail to identify a reasonable and consistent set of maxima and minima to which the local function can be fitted, especially for noisy or non-cleared seasonal data (Jonsson and Eklundh, 2002). To overcome these challenges, in the current research we used the SG filter to produce corrected VIs (termed NDVIsg and EVIsg) time series from the original MODIS VIs at 250 m resolution. The SG filter allows the removal of noise due to cloud contamination in the time series, while closely following sharp variations (the phenological signature) in the magnitude of the VI (16-day composites). The SG filter was initially and is still frequently used to make the relative widths and heights of spectral lines in noisy spectrometric data visible (William, 2007). It is also efficient in reducing contamination in VI time series caused primarily by cloud and atmospheric variability (Chen et al., 2004). The SG filter can be applied to smooth VI data sets sampled at various intervals such as daily, 10 day, or monthly (Chen et al., 2004).

In this study we investigate the appropriateness of using time-series data for the VIs derived from MODIS for land

cover classification and the effect of applying the SG filter on the time-series data and resulting classifications. Hence, the objectives of this study are to (a) apply the SG filter to reduce contamination in the VI time series and smooth out the temporal data, (b) assess the improvement in classification accuracy with the SG filter, and (c) statistically evaluate land cover classification using MODIS EVI and NDVI data (with and without the SG filter). Hence, this study identifies the optimal data form for land cover classification, using periodic data for land cover.

Materials and Methods

Study Area
The current research focuses over South Korea, in region situated within latitude 33°09' to 38°45'N and longitude 124°54' to 131°06'E with an approximate area of 96,070 km², where mountainous/hilly terrain represents approximately 64 percent of this area (Figure 1a). The mean elevation and slope are 433 m and 10.4 percent, respectively. The Taebaek Sanmaek (Taebaek Mountain Range) rises to over 1,500 m on the eastern side of the peninsula and drops abruptly toward the East Sea with little or no coastal plains. In the central zone, moderately high mountains dominate the landscape,

however, lowlands are found mainly along the western side of the peninsula, and extensive lowlands are present in the south (The National Atlas of Korea). Land cover data was produced based on 1 m × 1 m airborne image and field survey (Ministry of Environment, 2008). It is composed of needle-leaf forests (32 percent, mainly *Pinus densiflora*), broad-leaf forests (17 percent, mainly *Quercus* spp.), mixed forests (19 percent, needle-leaf and broad-leaf), cropland (25 percent), and urban areas (7 percent) (Figure 1b). South Korea has a temperate climate with four distinct seasons where the annual average temperature varies from 10° to 16°C, except in the hilly regions and annual precipitation of about 1,500 mm.

MODIS VIs Data
Twelve-month time series of 16-day composite Terra MODIS 250 m EVI and NDVI data (MOD13Q1 v004) spanning one growing season (January to December 2008) were produced for South Korea. The data (MOD13Q1) were downloaded from the Distribution Active Archive Center at NASA Goddard Space Flight Center. Both time series consisted of 23 data files, with each file a 16-day composite. The EVI and NDVI data were extracted from the MODIS tile (h28v05) and reprojected to the Universal Transverse Mercator (UTM) then compared to field sites with specific land cover types.

TABLE 1. THE RANGES AND MAJOR CHARACTERISTICS OF THE VIS FOR EACH CLASS

Class	EVI		NDVI	
	Range	High value composite	Range	High value composite
Needle-leaved	0.10 – 0.55	9th – 17th (27 May – 02 October)	0.25 – 0.90	8th – 19th (11 May – 04 November)
Broad-leaved	0.10 – 0.78	10th – 18th (12 June – 18 October)	0.15 – 0.97	9th – 18th (27 May – 18 October)
Mixed	0.10 – 0.65	9th – 18th (27 May – 18 October)	0.29 – 0.92	8th – 19th (11 May – 04 November)
Crop	0.10 – 0.7	12th – 18th (14 July – 18 October)	0.2 – 0.9	12th – 18th (14 July – 18 October)
Urban	<0.2	-	<0.4	-

Figure 1. (a) The study area - South Korea, and (b) The occupation percentage of land cover types (needle, broad, crop, urban, and mixed) in South Korea.
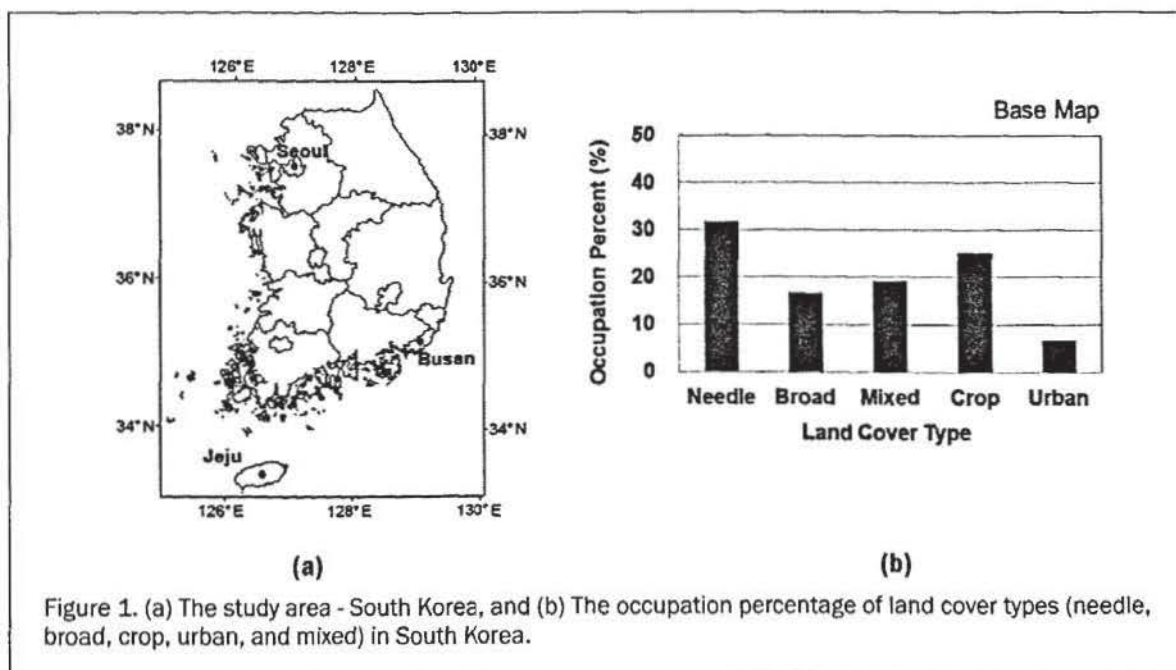
The NDVI is a normalized difference measure comparing the near infrared and visible red bands shown in Equation 1 (Rouse et al., 1973; Tucker et al., 1991):

$$NDVI = \frac{\rho_{NIR} - \rho_{red}}{\rho_{NIR} + \rho_{red}} \qquad (1)$$

where ρ_{red} and ρ_{NIR} represent the surface reflectance of the MODIS red band (620–670 nm) and the NIR band (871–876 nm), respectively.

The EVI is a modified NDVI with a soil adjustment factor L and two coefficients, C_1 and C_2, which describe the use of the blue band to correct the red band for atmospheric aerosol scattering as shown in Equation 2:

$$EVI = G \frac{(\rho_{NIR} - \rho_{red})}{(\rho_{NIR} + c_1 \times \rho_{red} - c_2 \times \rho_{blue} + L)} \qquad (2)$$

where ρ_{blue} is the blue band (459–479 nm). The coefficients C_1, C_2, and L have been empirically determined to be 6.0, 7.5, and 1.0, respectively, and G is set to be 2.5 as a gain factor. Such modification improves sensitivity to high-biomass regions and vegetation monitoring through decoupling of the canopy background signal and reduction in atmospheric influences (Huete et al., 2002).

Seasonal and monthly cycles of MODIS-derived Aerosol Optical Depth (AOD) over East Asia show a maximum in spring and a minimum in autumn and winter (Kim et al., 2007). For our purpose the EVI product has improved sensitivity over high biomass regions and improved vegetation monitoring capability through a de-coupling of the canopy background signal and a reduction in atmosphere influences. Hence, EVI data should be more suitable than NDVI (Xiao et al., 2003), as we were using the temporal signature of each class over an entire year, and the EVI uses the blue band to account for the atmospheric aerosols, hence the EVI is less affected (Xiao et al., 2003), which is particularly important during the spring.

The Savitzky-Golay Filter Algorithm

Savitzky and Golay (1964) proposed a polynomial function-fitting method based on a weighted least squares regression approach. This approach tends to preserve features of the data set such as relative maxima, minima, and widths. The filter could be viewed as a weighted moving average filter with weighting given as a polynomial of a certain degree. This filter can be applied to any consecutive data when the data points are located at fixed and uniform intervals along the chosen abscissa. The curve formed by graphing the points must be continuous and more or less smooth. In this study, the consecutive points were VI values at regular intervals (every 16 days). VI values (MOD13Q1 data) are distributed in 16-day composites, which do not mean that the data for any given pixel occurred on a regular frequency of 16 days. However, in this study, SG filter is used to find out its impact on time series data. The filter algorithm is as follows:

$$Y_j^* = \frac{\sum_{i=-m}^{i=m} C_i \times Y_{j+i}}{N} \qquad (3)$$

where, Y is the original VI value, Y_j^* is the filtered VI value, C_i is the coefficient for the ith VI value of the filter (smoothing window), and N is the number of convoluting integers equal to the smoothing window size ($2m + 1$). The index j is a running index of the original ordinate data table. The smoothing array (filter size) consists of $2m + 1$ points, where m is the half-width of the smoothing window. A larger value of m produces a smoother result at the expense of flattening sharp peaks.

The SG filter constitutes the core of a workflow used to process VI time-series data according to the method proposed by Chen et al. (2004). First, cloudy values within a time profile are identified based on information from the MOD13Q1 data set. These values are replaced by a linear interpolation of the nearest cloud-free neighboring values. Second, the SG filter is applied to calculate a set of smoothed time series data points using different weighting options. Third, it calculates weights for iterative filtering based on the long-term change trend and the preprocessed time profile. The final filtering process then uses the initial curve, the change trend and the weights to calculate a new curve. The filtering process is terminated when the fitting effect index is minimized (Chen et al., 2004).

Land Cover Classification and Assessment

In the current research, land cover classification was performed over a two-step procedure. First, the representative training areas were identified and a numeric description of the spectral attributes of each land cover type in the scene was derived from the VI data set. Second, the maximum likelihood classification (MLC) was applied for each time-series set of filtered VI data. The MLC method assumes that the training data statistics for each class in the bands are normally distributed (Gaussian). Therefore, each pixel was assigned to the class with the highest probability (Jensen, 2011).

A database of 167 training areas with specific land cover types was created using information from aerial photos and field visits. The mean training area size was 442 ha, and sizes ranged from 48 to 1,545 ha depending on the land type. There was a large range of training area sizes because the areas were not spectrally homogeneous in the high spatial resolution imagery, although they were naturally homogeneous.

Classification results were verified using land cover ratio of each class by Ministry of Environment (2008) and independent reference data (test areas), where 552 test area locations were randomly and independently selected for each classification class. We performed visual interpretation of the aerial photos to identify potential accuracy assessment areas and investigated each of these areas in the field. Producer's and user's accuracy (Congalton and Green, 2009; Story and Congalton, 1986) verification was performed using cross tabulation and the Kappa value ($\hat{K}$).

$\hat{K}$ is a measure of agreement or accuracy between the remote sensing-derived classification map and the reference data (Congalton, 1991; Swets et al., 1999). The $\hat{K}$ function is calculated as follows:

$$\hat{K} = \frac{N \sum_{i=1}^{K} x_{ii} - \sum_{i=1}^{K} (x_{i+} \times x_{+i})}{N^2 - \sum_{i=1}^{K} (x_{i+} \times x_{+i})} \qquad (4)$$

where k is the number of rows (land cover classes) in the matrix, x^{ii} is the number of observations in row i and column i, x_{i+} and x_{+i} are the marginal totals for row i and column i, respectively, and N is the total number of observations. $\hat{K}$ values >0.80 represent strong agreement or accuracy between the classification map and the ground reference information. $\hat{K}$ values ranging from 0.40 to 0.80 represent moderate agreement. $\hat{K}$ values <0.40 represent poor agreement (Landis and Koch, 1977).

Results and Discussion

Determination of the Corrected Vegetation Indices

The EVI is nearly always lower than the NDVI throughout the EVI/NDVI range of values (0 to 1.0; Terrestrial Biophysics and Remote Sensing Lab, 2008). The NDVI temporal profiles show anomalous drops in the VI, particularly during the 13th composite (30 July) compared to the 12th and 14th composite.

This drop is conspicuous in both the needle- and broad-leaf classes (Figure 2). It is well known that the growing season of vegetation in Korea is from April to October and growth peaks would be different between species. However, although July is within the growing season for needle- and broad-leaf trees, anomalous declines appear during this period (Figure 2). These anomalies during July can be attributed to a number of potential factors, such as cloud contamination, large atmospheric variability, and bi-directional effects. Such disturbances in space-based VI measurements, particularly during the summer rainfall season, greatly affect monitoring of land cover and terrestrial ecosystems and act as undesirable noise (Cihlar et al., 1997). Therefore, it is clear that almost all sudden dips that occur in growing season could be considered as noise that is corrected in the time series using the SG filter. Therefore, we applied the SG filter to smooth out the time series and remove undesirable noise such as these large anomalous drops seen in the VI values. The EVIsg and NDVIsg time-series profiles clearly show the positive effect of time-series smoothing, in which outliers are fitted to the long-term
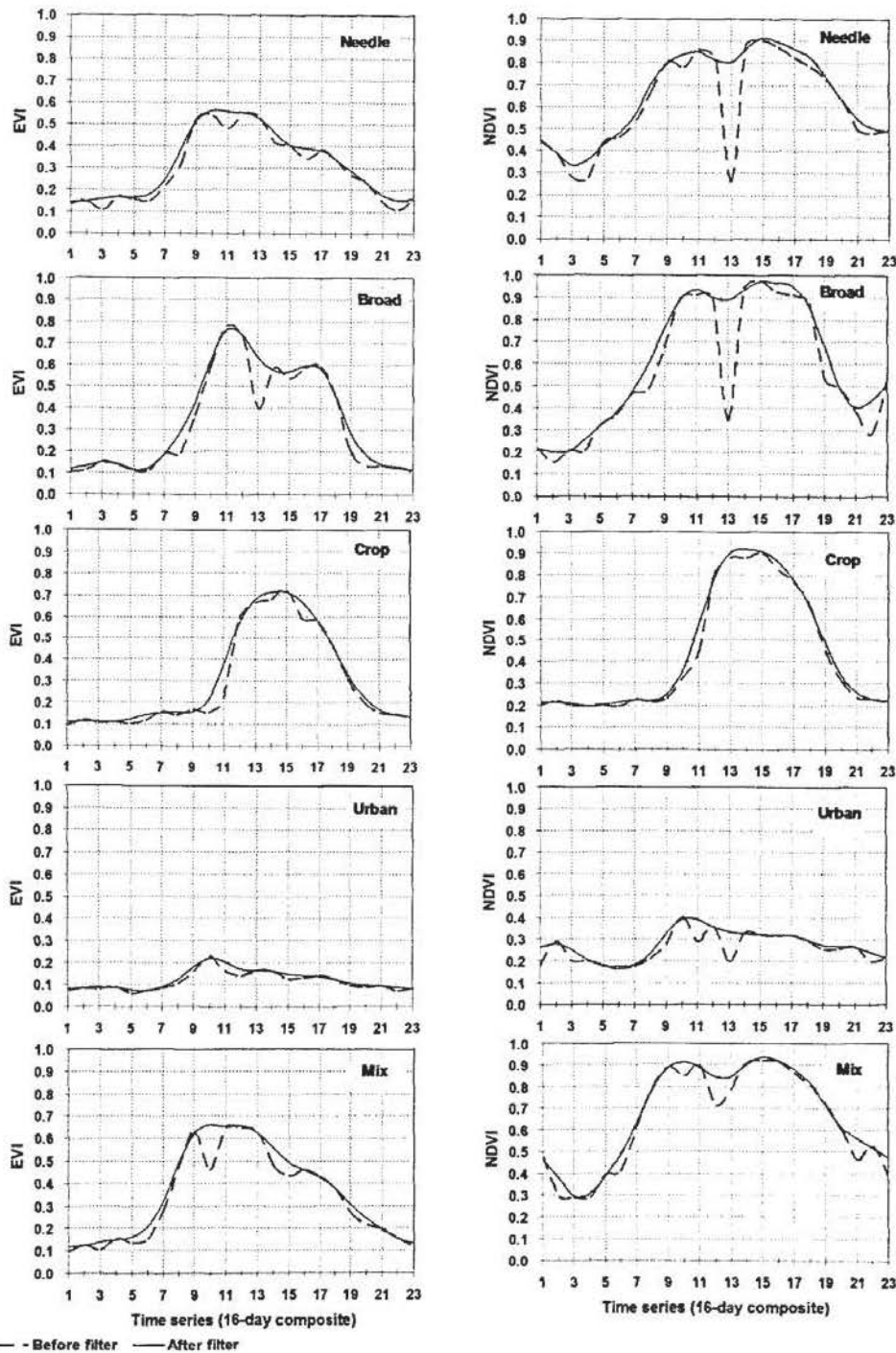
Figure 2. The left column shows the original EVI (dashed line) and SG-filtered EVI (EVIsg, solid line), and the right column shows the original NDVI (dashed line) and the SG-filtered NDVI (NDVIsg, solid line) temporal signature for the various land cover classes (needle, broad, crop, urban, and mixed) for 2008. The numbers on the x-axis correspond to the sequential numbering (1 through 23) of the 16-day MODIS composites for January to December 2008.
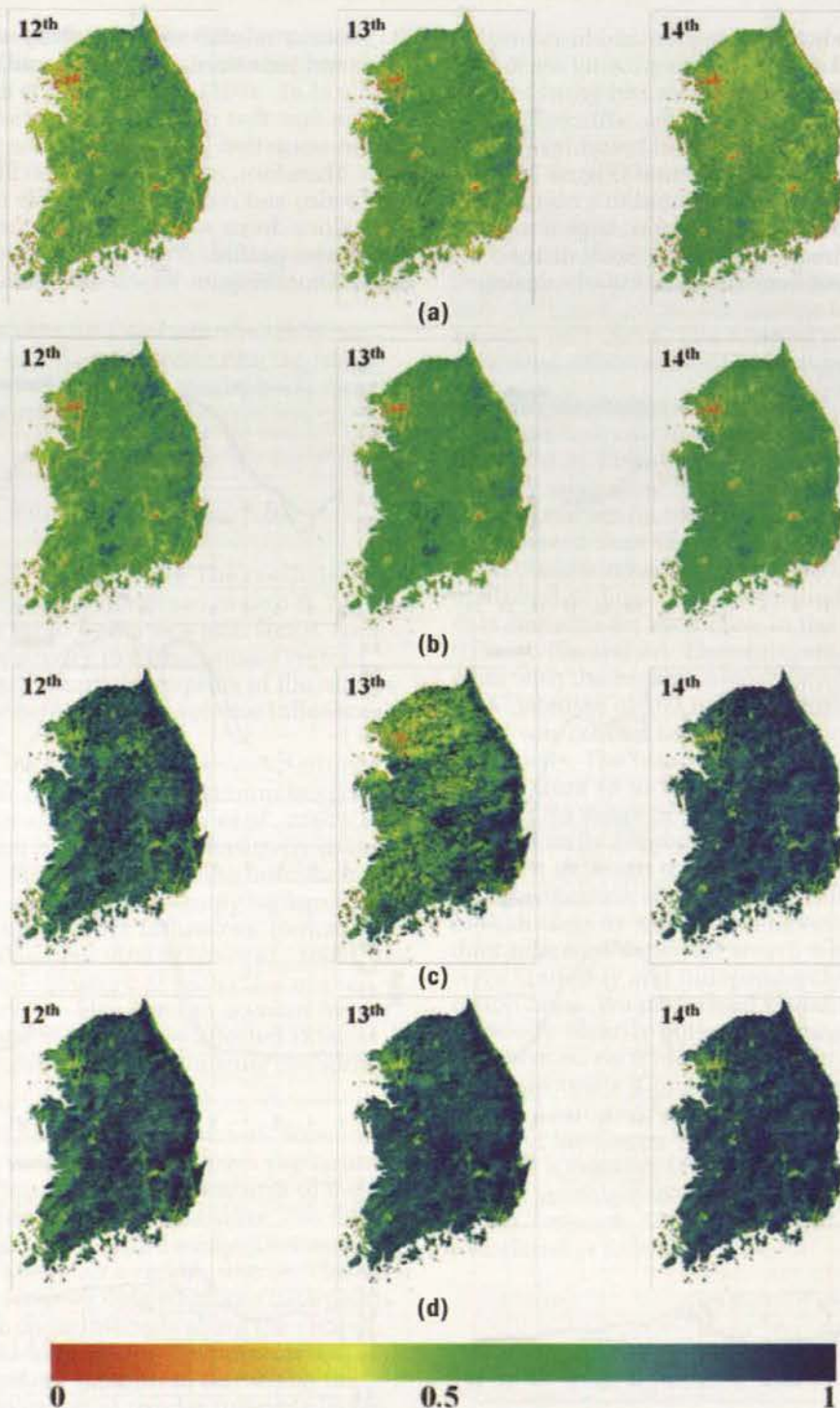
Plate 1. (a) The original EVI image (before the SG filter, EVI), (b) the corrected EVI image (after the SG filter, EVIsg), (c) the original NDVI image (before the SG filter, NDVI), and (d) the corrected NDVI image (after the SG filter, NDVIsg) for three consecutive 16-day MODIS composites (12th, 13th, and 14th) during 2008 over South Korea.

curve trend for each class (Figure 2). The temporal profiles for the needle- and broad-leaf classes clearly show the effect of applying the SG filter to the MODIS time-series data.

Nonetheless, it is noteworthy that SG filter has a drawback of smoothing out the subtle details, however, phenomena occurrence and variability dependent on those little peaks and dips were out of our scope and not considered in this study. Thus, further study would be executed for overcome these shortcomings.

To explicitly test the spatial effect of the SG filter, a comparison of the NDVIs and EVIs with and without filtering is presented in Plate 1. The anomalous decline in the NDVI and EVI values in the 13th composite is corrected by applying the SG filter. Thus, the NDVIsg and EVIsg maps show smooth

transitions in the VI from the 12th to the 14th composite, unlike the original NDVI and EVI maps for the same period (Plate 1). The temporal profiles (Figure 2) and spatial maps (Plate 1) for the needle- and broad-leaf classes clearly show the effect of applying the SG filter to the MODIS time-series data.

Land Cover Classification and Accuracy Assessment

Plate 2a and 2b show the land cover classifications derived from the EVI and EVIsg time-series data. Land cover data provided by the Ministry of Environment was compared with that calculated from EVI, EVIsg, NVDI, and NDVIsg to find out area distribution difference. As a result we observed some changes in the actual land cover fractions (Figure 1b), as follows. EVI- and EVIsg-derived needle-leaf class fractions (38 percent and 37
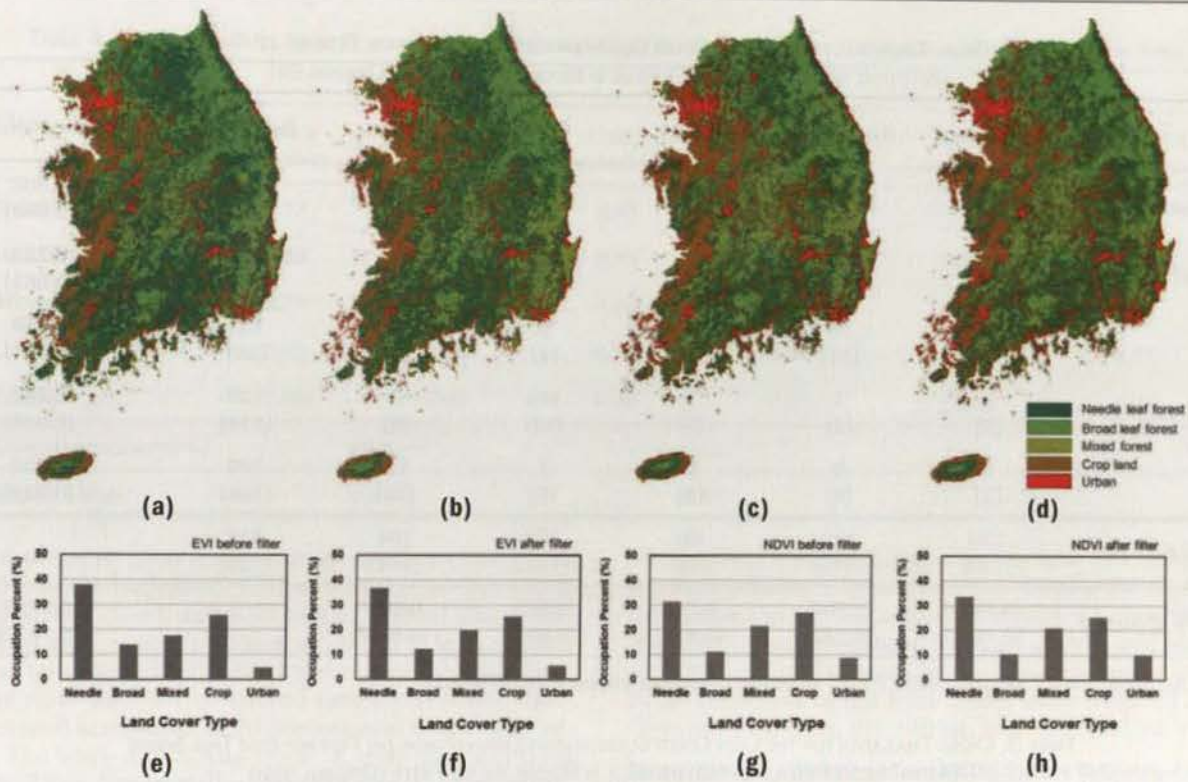
Plate 2. The top panel shows land cover maps derived from (a) the original EVI time series before the SG filter, (b) the EVISG time series after the SG filter, (c) the original NDVI time series before the SG filter, and (d) the NDVISG time series after the SG filter. The bottom panel shows the corresponding land cover class percentages (e) using EVI, (f) using EVISG, before and after the SG filter, respectively, and (g) using NDVI, and (h) using NDVISG, before and after the SG filter, respectively.
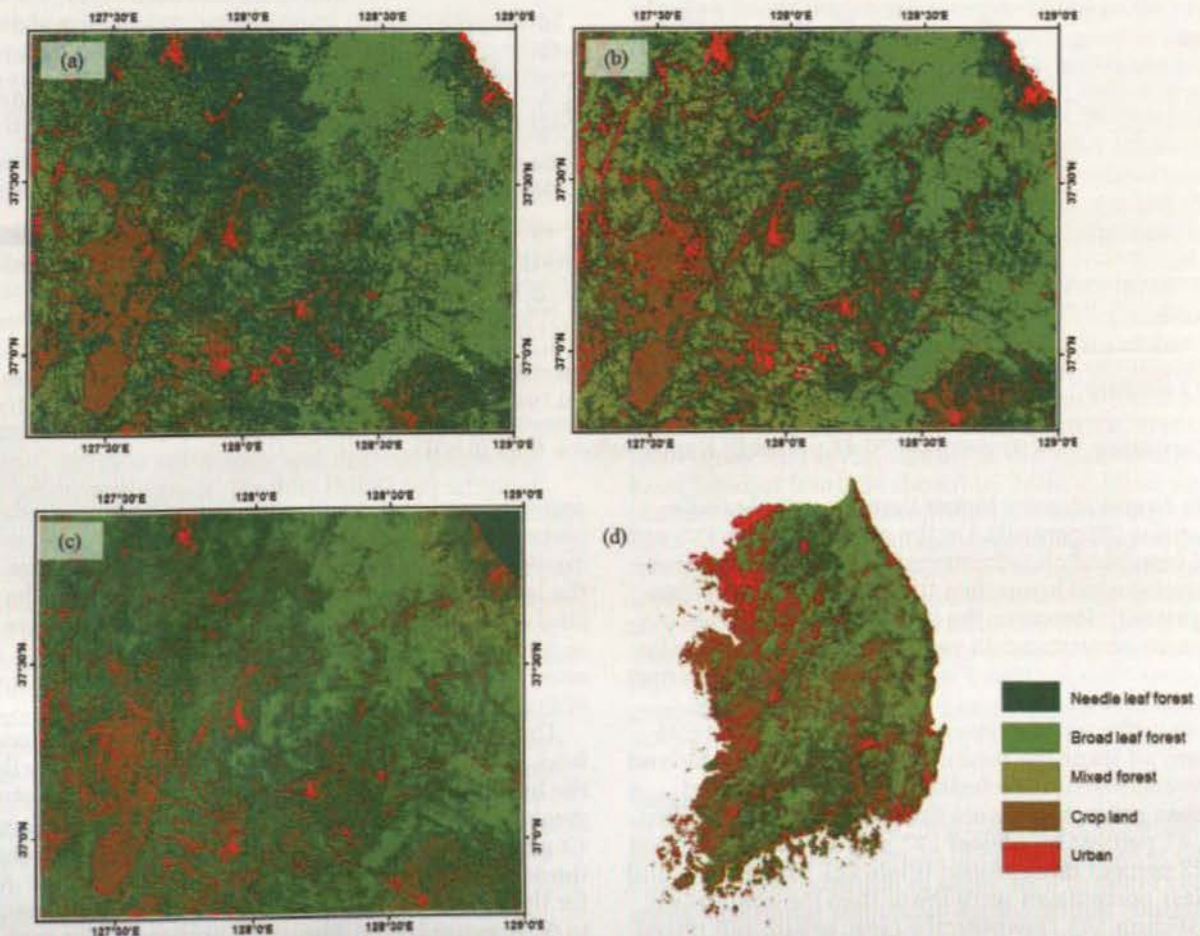
Plate 3. Land cover classification maps derived from multi-temporal data: (a) Eves, (b) NDVISG, (c) a multi-band Landsat image (see Table 4), and (d) a multi-band MODIS image (see Table 5).

TABLE 2. CROSS TABULATION FOR THE LAND COVER CLASSIFICATION DERIVED FROM THE FILTERED EVI TIME SERIES (AFTER THE SG FILTER, EVISG); ( ) VALUE IS BEFORE THE SG FILTER (ORIGINAL EVI)

Class	Needle-leaf	Broad-leaf	Mixed	Crop	Urban	Row total	User's accuracy
Needle- leaf	93 (97)	7 (9)	9 (22)	5 (11)	2 (3)	116 (142)	0.802 (0.683)
Broad- leaf	15 (15)	77 (82)	13 (25)	0 (0)	0 (2)	105 (124)	0.733 (0.661)
Mixed	14 (11)	18 (11)	63 (39)	6 (4)	1 (1)	102 (66)	0.618 (0.591)
Crop	5 (5)	2 (2)	1 (0)	104 (98)	8 (9)	120 (114)	0.867 (0.860)
Urban	3 (2)	6 (6)	0 (0)	7 (9)	93 (89)	109 (106)	0.853 (0.840)
Column total	130 (130)	110 (110)	86 (86)	122 (122)	104 (104)	552 (552)	
Producer's accuracy	0.715 (0.746)	0.700 (0.745)	0.733 (0.453)	0.852 (0.803)	0.894 (0.856)		0.7790 (0.7337)

Overall accuracy = 77.90 percent (73.37 percent), Kappa value = 0.72 (0.67)

TABLE 3. CROSS TABULATION FOR THE LAND COVER CLASSIFICATION DERIVED FROM THE FILTERED NDVI TIME SERIES (AFTER THE SG FILTER, NDVISG); ( ) VALUE IS BEFORE THE SG FILTER (ORIGINAL NDVI)

Class	Needle-leaf	Broad-leaf	Mixed	Crop	Urban	Row total	User's accuracy
Needle- leaf	90 (79)	10 (7)	24 (18)	12 (10)	1 (3)	137 (117)	0.657 (0.675)
Broad- leaf	10 (12)	60 (66)	16 (12)	0 (0)	0 (0)	86 (90)	0.698 (0.733)
Mixed	20 (22)	31 (30)	45 (53)	1 (2)	1 (1)	98 (108)	0.459 (0.491)
Crop	8 (11)	3 (1)	1 (3)	94 (97)	5 (6)	111 (118)	0.847 (0.822)
Urban	2 (6)	6 (6)	0 (0)	15 (13)	97 (94)	120 (119)	0.808 (0.790)
Column total	130 (130)	110 (110)	86 (86)	122 (122)	104 (104)	552 (552)	
Producer's accuracy	0.692 (0.608)	0.545 (0.600)	0.523 (0.616)	0.770 (0.795)	0.933 (0.904)		0.6993 (0.7047)

Overall accuracy = 69.93 percent (70.47 percent), Kappa value = 0.62 (0.63)

percent; Plate 2e and 2f) were higher than the actual needle-leaf class fractions (32 percent). On the other hand, the EVI- and EVIsg-derived broad-leaf class fractions (14 percent and 12 percent, respectively) were lower than the actual broad-leaf class fraction (17 percent). However, the EVI and EVIsg crop class fractions were 26 percent and 25 percent, respectively, similar to the actual crop class fraction. Finally, the EVI and EVIsg urban class fractions were 5 percent and 6 percent, respectively, much lower than the actual urban class fraction (19 percent).

Plate 2c and 2d show the land cover classifications derived from the NDVI and NDVIsg time series data. The NDVI-based land cover class percentages were distributed into 31 percent needle-leaf , 11 percent broad-leaf , 27 percent crop, 9 percent urban, and 22 percent mixed forest (Plate 2g). The needle- and broad-leaf class percentages were lower than the actual class percentages (Figure 1b). However, the crop, urban, and mixed forest class percentages were higher than the actual class percentages. On the other hand the NDVIsg-based land cover class percentages were distributed into 34 percent needle-leaf , 10

percent broad-leaf, 25 percent crop, 10 percent urban, and 21 percent mixed forest (Plate 2h). The needle-leaf, urban, and mixed forest class percentages were higher (Figure 1c), while the broad-leaf class percentage was lower, than the actual land cover percentages. The crop class percentages were same in both cases. Hence, the EVIsg-based classification result has most similar value with land cover that provided by Ministry of Environment (Table 1).

Cross tabulation for the land cover classifications derived from the EVI and EVIsg is shown in Table 2, where the value in the brackets represents value of original EVI. We observed a great improvement in the overall classification accuracy from 73 percent for the EVI to 78 percent for the EVIsg after applying the SG filter to the EVI data. Hence, the calculated $\hat{K}$ values for the EVI- and EVIsg-based classifications improved from 0.67 to 0.72, respectively. The user's accuracies for each class, a measure of the reliability of the output map based on the classification scheme, showed significant improvements for the EVIsg-based classification compared with that for the EVI.

TABLE 4. ACCURACY OF LAND COVER CLASSIFICATIONS DERIVED FROM TIME-SERIES DATA (EVISG, NDVISG) AND A MULTI-BAND LANDSAT IMAGE

Class	EVIsg		NDVIsg		Landsat	
	User's accuracy	Producer's accuracy	User's accuracy	Producer's accuracy	User's accuracy	Producer's accuracy
Needle-leaf	0.73	0.60	0.73	0.60	0.58	0.41
Broad-leaf	0.68	0.87	0.73	0.76	0.63	0.87
Mixed	0.77	0.62	0.56	0.68	0.50	0.29
Crop	0.93	0.82	0.77	0.63	0.77	0.77
Urban	1.00	1.00	0.50	1.00	0.60	1.00
Overall accuracy (%)	74.2		68.5		62.1	
Kappa value	0.64		0.57		0.47	

Application of the SG filter increased the user's accuracy from 0.68 to 0.80 (needle-leaf class), 0.66 to 0.73 (broad-leaf class), 0.84 to 0.85 (urban class), and 0.59 to 0.62 (mixed class). The crop class had similar user's accuracy (~0.86) in both cases.

The cross tabulation for the NDVI and NDVIsg is shown in Table 3. The NDVI- and NDVIsg-derived land cover classifications had overall accuracies of 70 percent and 69 percent, respectively. The NDVI- and NDVIsg-based $\hat{K}$ were 0.63 and 0.62, respectively. Thus, the overall accuracies and $\hat{K}$ values for the NDVI- and NDVIsg-derived land cover classifications were similar. The user's accuracies for the NDVI- and NDVIsg-based classifications had mixed results. The user's accuracies for the crop and urban classes improved for the NDVIsg-based classification over the NDVI-based classification.

Therefore in conclusion, we observed that the EVIsg-based classification had better user's accuracy for all individual classes than the EVI-, NDVI-, or NDVIsg-based classifications (Tables 2 and 3). The accuracy analysis clearly indicates that the EVIsg time-series data is the most suitable for achieving the highest overall classification accuracy as well as individual class user's accuracy compared to other data sets (EVI, NDVI, and NDVIsg).

Comparison with a Multi-band Landsat Surface Reflectance Image
Plate 3 shows a comparison of land cover classification maps derived from multitemporal data (EVIsg, NDVIsg) (Plate 3a and 3b) with that from a multi-band Landsat-7 ETM+ (Enhanced Thematic Mapper Plus) surface reflectance image (Plate 3c). The Landsat data, used for land cover classification, consists of seven surface reflectance bands ranging from visible to near infrared (NIR), shortwave infrared (SWIR), and longwave infrared (LWIR). Surface reflectance was derived following the MODIS Surface-Reflectance Product (MOD 09) which is computed from the land bands 1, 2, 3, 4, 5, 6, and 7 (centered at 648 nm, 858 nm, 470 nm, 555 nm, 1240 nm, 1640 nm, and 2130 nm, respectively). The product is an estimate of the surface spectral reflectance for each band as it would have been measured at ground level if there were no atmospheric scattering or absorption. Since 2003 all Landsat ETM images have had wedge shaped gaps on both sides of each scene, resulting in approximately 22 percent data loss. Scaramuzza et al. (2004) developed a technique which can be used to fill gaps in one scene with data from another Landsat scene. A linear transform is applied to the "filling" image to adjust it based on the standard deviation and mean values of each band, of each scene. We have used the 07 May 2008 Landsat data in this study to satisfy the best period (early-May) most suitable to distinguish vegetation types in Korea. We encountered a problem of scene absence at same period from Landsat-7 ETM+, and therefore, the scene which has enough information needed in this study was selected and used. Classification

results were verified using only the new 124 test area independent reference data. However, despite the high spatial resolution (30 m), the overall accuracy was low (62.1 percent; $\hat{K} = 0.47$) when compared to those of EVIsg and NDVIsg (Table 4). Errors of commission due to mis-assignment of categories in the classified image were much more frequent for each class than for EVIsg, EVI, NDVIsg, and NDVI (Tables 2 and 3).

Comparison with a Multi-band Terra MODIS Surface Reflectance Image
Plates 2 and 3 show a comparison of land cover classification maps derived from multi-temporal data (EVIsg, NDVIsg) (Plate 2b and 2d) with that from a multi-band MODIS surface reflectance image (Plate 3d) at 500 m (Level 2G, dated 02 May 2008). The MODIS data, product code MOD09GA, consists of seven bands which are estimate of the surface spectral reflectance as it would be measured at ground level at various wavelengths. The surface reflectance bands used in classification are: Band 1 (620–670 nm), Band 2 (841–876 nm), Band 3 (459–479 nm), Band 4 (545–565 nm), Band 5 (1230–1250 nm), Band 6 (1628–1652 nm), and Band 7 (2105–2155 nm). A comparison of user's accuracy and producer's accuracy is shown in Table 5. The overall accuracy was low (57.6 percent; $\hat{K} = 0.47$) when a multi-band surface reflectance image from MODIS was used for classification. The overall and individual class accuracies (Table 5) were lower than those of Landsat as well as EVIsg, EVI, NDVI, and NDVIsg (Tables 2 and 3). The errors of commission were even higher than for Landsat due to increased mis-assignment of categories in the classified image.

In summary, a comparison of the accuracy of land cover classifications, over the same spatial extent, derived from time-series data (EVIsg, NDVIsg) to that derived from a multi-band Landsat image is shown in Table 4. Mis-assignment of classes, i.e., errors of commission, were the highest for the Landsat classification image when compared to the EVIsg and NDVIsg images (Table 4; Plate 3). The overall accuracy was lower (62.1 percent) for the Landsat classifications than those derived from EVIsg (74.2 percent) and NDVIsg (68.5 percent). Similarly, the overall accuracy was lower for classifications derived from multi-band Terra MODIS (57.6 percent) when compared to those derived from EVIsg (77.9 percent) and NDVIsg (69.9 percent) (Table 5; Plates 2 and 3).

Conclusions
In the present work, we investigated the applicability and potential advantages of the SG filter for land cover classification, as well as the reduction of noise such as cloud contamination, using time-series signatures for individual classes derived from MODIS 250 m VI data sets for South Korea. The phenological stages (signatures) for each ecosystem class were used for classification based on temporal variations in VIs over the

TABLE 5. ACCURACY OF LAND COVER CLASSIFICATIONS
DERIVED FROM A MULTI-BAND MODIS IMAGE

Class	MODIS (multi bands)	
	User's accuracy	Producer's accuracy
Needle- leaf	0.55	0.37
Broad- leaf	0.52	0.70
Mixed	0.41	0.35
Crop	0.65	0.66
Urban	0.70	0.80
Overall accuracy (%)	57.6	
Kappa value	0.47	

period of a year. We carried out land cover classification using a standard procedure with only a single multi-band image. The primary results include:

- The overall accuracies of land cover classifications based on the MLC method using EVI, EVIsg, NDVI, and NDVIsg were 73 percent, 78 percent, 70, and 70 percent, respectively. The calculated Kappa values ($\hat{K}$) for the land cover classifications using EVI, EVIsg, NDVI, and NDVIsg were 0.67, 0.72, 0.63, and 0.62, respectively.
- The cross tabulation analysis indicated that the SG-filtered EVI time series (EVIsg) was most suitable for classifying and delineating land cover compared to the original EVI and NDVI data sets or the SG-filtered NDVI (NDVIsg).
- The EVI corrected for aerosol effects using the blue band performed better than the NDVI, particularly over regions with relatively high aerosol loading.
- The SG filter further enhanced the accuracy of the land cover classifications by reducing noise sources through temporal smoothing of the time-series signatures for each class.
- The overall accuracy of the classifications based on multi-band Landsat and Terra MODIS were 62.1 percent and 57.6 percent, respectively, substantially lower than that of EVIsg.
- The phenological signature of an individual ecosystem class is an intrinsic advantage of using time-series data and yields better classification maps than single multi-band (surface reflectance) composites such as those from Landsat and MODIS.

The present study classified land cover by large scale into four different classes namely, needle-leaf, broad- leaf, mixed, crop and urban class using temporal VI and found the optimal data form to land cover classification. Thus, we conclude that the SG-filtered EVI (EVIsg) is the most accurate and appropriate methodology for carrying out time series-based land cover classification among the MODIS vegetation data sets (EVI, NDVI, NDVIsg) and also compared to single-date multi-band surface reflectance images from Landsat and Terra MODIS.

References

Bakr, N., D.C. Weindorf, M.H. Bahnassy, S.M. Marei, and M.M. El-Badawi, 2010. Monitoring land cover changes in a newly reclaimed area of Egypt using multi-temporal Landsat data, *Applied Geography*, 30(4):592–605.

Carvalho, L.M.T., J.G.P.W. Clevers, A.K. Skidmore, and S.M. de Jong, 2004. Selection of imagery data and classifiers for mapping Brazilian semideciduous Atlantic forests, *International Journal of Applied Earth Observation and Geoinformation*, 5(3):173–186.

Chen, J., P. Jonsson, M. Tamura, Z. Gu, B. Matsushita, and L. Eklundh, 2004. A simple method for reconstructing a high-quality NDVI time-series data set based on the Savitzky-Golay filter, *Remote Sensing of Environment*, 91(3-4):332–344.

Cihlar, J., 2000. Land-cover mapping of large areas from satellites: Status and research priorities, *International Journal of Remote Sensing*, 21(6-7):1093–1114.

Cihlar, J., H. Ly, Z.Q. Li, J. Chen, H. Pokrant, and F.T. Huang, 1997. Multitemporal, multichannel AVHRR data sets for land biosphere studies-artifacts and corrections, *Remote Sensing of Environment*, 60(1):35–57.

Congalton, R., and K. Green, 2009. *Assessing the Accuracy of Remotely Sensed Data: Principles and* Practices, Second edition, CRC/Taylor & Francis, Boca Raton, Florida, 183 p.

Congalton, R.G., 1991. A review of assessing the accuracy of classifications of remotely sensed Data, *Remote Sensing of Environment*, 37(1):35–46.

Dash, J., A. Mathur, G.M. Foody, P.J. Curran, J.W. Chipman, and T.M. Lillesand, 2007. Land cover classification using multi-temporal MERIS vegetation indices, *International Journal of Remote Sensing*, 28(6):1137–1159.

de Jong, R., S. de Bruin, A. de Wit, M.E. Schaepman, and D.L. Dent, 2011. Analysis of monotonic greening and browning trends from global NDVI time-series, *Remote Sensing of Environment*, 115(2):692–702.

Doraiswamy, P.C., T.R. Sinclair, S. Hollinger, B. Akhmedov, A. Stern, and J. Prueger, 2005. Application of MODIS derived parameters for regional crop yield assessment, *Remote Sensing of Environment*, 97(2):192–202.

Esquerdo, J.C.D.M., J. Zullo Jr., and J.F.G. Antunes, 2011. Use of DVI/AVHRR time-series profiles for soybean crop monitoring in Brazil, *International Journal of Remote Sensing*, 32(12):3711–3727.

Fischer, A., 1994. A model for the seasonal variations of vegetation indices in coarse resolution data and its inversion to extract crop parameters, *Remote Sensing of Environment*, 48(2):220–230.

Friedl, M.A., D.K. McIver, J.C.F. Hodges, X.Y. Zhang, D. Muchoney, A.H. Strahler, C.E. Woodcock, S. Gopal, A. Schneider, A. Cooper, A. Baccini, F. Gao and C. Schaaf, 2002. Global land cover mapping from MODIS: Algorithms and early results, *Remote Sensing of Environment*, 83:287–302.

Galford, G.L., J.F. Mustard, J. Melillo, A. Gendrin, C.C. Cerri, and C.E.P. Cerri, 2008. Wavelet analysis of MODIS time series to detect expansion and intensification of row-crop agriculture in Brazil, *Remote Sensing of Environment*, 112(2):576–587.

Gu, J., X. Li, C. Huang, and G.S. Okin, 2009. A simplified data assimilation method for reconstructing time-series MODIS NDVI data, *Advances in Space Research*, 44(4):501–509.

Heinl, M., J. Walde, G. Tappeiner, and U. Tappeiner, 2009. Classifiers vs. input variables - The drivers in image classification for land cover mapping, *International Journal of Applied Earth Observation and Geoinformation*, 11(6):423–430.

Herold, M., P. Mayaux, C.E. Woodcock, A. Baccini, and C. Schmulliu, 2008. Some challenges in global land cover mapping: An assessment of agreement and accuracy in existing 1 km datasets, *Remote Sensing of Environment*, 112(5):2538–2556.

Hird, J.N., and G.J. McDermid, 2009. Noise reduction of NDVI time series: An empirical comparison of selected techniques, *Remote Sensing of Environment*, 113(1):248–258.

Homer, C., C.Q. Huang, L.M. Yang, B. Wylie, and M. Coan, 2004. Development of a 2001 national land-cover database for the United States, *Photogrammetric Engineering & Remote Sensing*, 70(7):829–840.

Huete, A.R., K. Didan, T. Miura, E.P. Rodriguez, X. Gao, and G. Ferreira, 2002. Overview of the radiometric and biophysical performance of the MODIS vegetation indices, *Remote Sensing of Environment*, 83(1-2):195–213.

Jensen, J.R., 2011. *Introductory Digital Image Processing: A Remote Sensing Perspective*, Third Edition, Prentice-Hall, London, pp. 374–379.

Jia, Y., C.L. Zhao, L. Zhou, and B. Niu, 2009. Estimation of leaf area index using remote sensing in the groundwater-fluctuating belt in lower reaches of Heihe River, Northwest China, *Proceedings of the 2009 International Conference on Environmental Science and Information Application Technology*, 3:462-465.

Jonsson, P., and L. Eklundh, 2002. Seasonality extraction by function fitting to time series of satellite sensor data, *IEEE Transactions on Geoscience and Remote Sensing*, 40(8):1824–1832.

Justice, C.O., and J.R.G. Townshend, 2002. Special issue on the Moderate Resolution Imaging Spectroradiometer (MODIS): A new generation of land surface monitoring, *Remote Sensing of Environment*, 83(1-2):1–2.

Kim, S.W., S.C. Yoon, J. Kim, and S.Y. Kim, 2007. Seasonal and monthly variations of columnar aerosol optical properties over east Asia determined from multi-year MODIS, LIDAR, and AERONET sun/sky radiometer measurements, *Atmospheric Environment*, 41(8):1634–1651.

Knight, J.F., and R.S. Lunetta, 2003. An experimental assessment of minimum mapping unit variability, *IEEE Transactions on Geoscience and Remote Sensing*, 41(9):2132–2134.

Knight, J.F., and R.S. Lunetta, 2006. Regional scale land cover characterization using MODIS NDVI 250 m multi-temporal imagery: A phenology-based approach, *GIScience and Remote Sensing*, 43(1):1–23.

Landis J., and G. Koch, 1977. The measurement of observer agreement for categorical data, *Biometrics*, 33(1):159–174.

Lovell, J.L., and R.D. Graetz, 2001. Filtering pathfinder AVHRR land NDVI data for Australia, *International Journal of Remote Sensing*, 22(13):2649–2654.

Lunetta, R.S., J.F. Knight, J. Ediriwickrema, J.G. Lyon, and L.D. Worthy, 2006. Land cover change detection using multi-temporal MODIS NDVI data, *Remote Sensing of Environment*, 105:142–154.

Marland, G., R.A. Pielke Sr., M. Apps, R. Avissar, R.A. Betts, K.J. Davis, P.C. Frumhoff, S.T. Jackson, L.A. Joyce, P. Kauppi, J. Katzenberger, K.G. MacDicken, R. Neilson, J.O. Niles, D.S. Niyogi, R.J. Norby, N. Pena, N. Sampson, and Y. Xue, 2003. The climatic impacts of land surface change and carbon management, and the implications for climate-change mitigation policy, *Climate Policy*, 3(2):149–157.

Myneni, R.B., S. Hoffman, Y. Knayzikhin, J.L. Privette, J. Glassy, Y. Tian, Y. Wang, X. Song, Y. Zhang, G.R. Smith, A. Lotsch, M. Friedl, J.T. Morisette, P. Votava, R.R. Nemani, and S.W. Running, 2002. Global products of vegetation leaf area and fraction absorbed PAR from year one of MODIS data, *Remote Sensing of Environment*, 83:214-231.

Oliveira, T.C.D., L.M.T. de Carvalho, L.T. de Oliveira, A.Z. Martinhago, F.W. Acerbi, and M.P. de Lima, 2010. Mapping deciduous forests by using time series of filtered MODIS NDVI and neural networks, *Cerne*, 16(2):123–130.

Roerink, G.J., M. Menenti, and W. Verhoef, 2000. Reconstructing cloud free NDVI composites using Fourier analysis of time series, *International Journal of Remote Sensing*, 21(9):1911–1917.

Rouse, J.W., R.H. Haas, J.A. Schell, and D.W. Deering, 1973. Monitoring vegetation systems in the Great Plains with ERTS, *Proceedings of the Third Earth Resources Technology Satellite-1 Symposium*, 10–14 December, Washington, D.C. (NASA, Goddard Space Center, Greenbelt, Maryland), pp. 309–317.

Samaniego, L., and K. Schulz, 2009. Supervised classification of agricultural land cover using a modified k-NN technique (MNN) and Landsat remote sensing imagery, *Remote Sensing*, 1(4):875–895.

Savitzky, A., and M.J.E. Golay, 1964. Smoothing and differentiation of data by simplified least squares procedures, *Analytical Chemistry*, 36(8):1627–1639.

Scaramuzza, P., E. Micijevic, and G. Chander, 2004. SLC gap-filled products: Phase one methodology, *http://www.ga.gov.au/webtemp/image_cache/GA4861.pdf* (last date accessed: 28 April 2014).

Story, M., and R.G. Congalton, 1986. Accuracy assessment: A user's perspective, *Photogrammetric Engineering & Remote Sensing*, 52(3):397–399.

Sulla-Menashe, D., M.A. Friedl, O.N. Krankina, A. Baccini, C.E. Woodcock, A. Sibley, G. Sun, V. Kharuk, and V. Elsakov, 2011. Hierarchical mapping of northern Eurasian land cover using MODIS data, *Remote Sensing of Environment*, 115(2):392–403.

Swets, D.L., B.C. Reed, J.R. Rowland, and S.E. Marko, 1999. A weighted least-squares approach to temporal smoothing of NDVI, *Proceedings of the 1999 ASPRS Annual Conference*, 17-21 May, Portland, Oregon, (American Society for Photogrammetry and Remote Sensing, Bethesda, Maryland), unpaginated CD-ROM.

Tucker, C.J., W.W. Newcomb, S.O. Los, and S.D. Prince, 1991. Mean and inter-year variation of growing-season normalized difference vegetation index for the Sahel 1981-1989, *International Journal of Remote Sensing*, 12(6):1113–1115.

Verhoef, W., M. Menentl, and S. Azzall, 1996. A color composite of NOAAAVHRR based on time series (1981-1992), *International Journal of Remote Sensing*, 17(2):231–235.

Verstraete, M.M., and B. Pinty, 1996. Designing optimal spectral indexes for remote sensing applications, *IEEE Transactions on Geoscience and Remote Sensing*, 34(5):1254–1265.

Viovy, N., O. Arino, and A.S. Belward, 1992. The best index processes extraction (BISE): A method for reducing noise in NDVI time series, *International Journal of Remote Sensing*, 13(8):1585–1590.

Wardlow, B.D., S.L. Egbert, and J.H. Kastens, 2007. Analysis of time-series MODIS 250m vegetation index data for crop classification in the U.S. central Great Plains, *Remote Sensing of Environment*, 108(3):290–310.

Wessels, K.J., R.S. De Fries, J. Dempewolf, L.O. Anderson, A.J. Hansen, S.L. Powell, and E.F. Moran, 2004. Mapping regional land cover with MODIS data for biological conservation: Examples from the greater Yellowstone ecosystem, *Remote Sensing of Environment*, 92(1):67–83.

William, H., 2007. *The Art of Scientific Computing*, Cambridge University Press, New York, New York, pp. 650–655.

Wu, C., Z. Niu, and S. Gao, 2010. Gross primary production estimation from MODIS data with vegetation index and photosynthetically active radiation in maize, *Journal of Geophysical Research*, 115:D12127 (11).

Xia, Z., S. Rui, Z. Bing, and T. Qingxi, 2008. Land cover classification of the North China Plain using MODIS_EVI time series, *ISPRS Journal of Photogrammetry and Remote Sensing*, 63(4):476–484.

Xiao, X., B. Braswell, Q. Zhang, S. Boles, S. Frolking, and B. Moore, 2003. Sensitivity of vegetation indices to atmospheric aerosols: Cntinental-scale observations in Northern Asia, *Remote Sensing of Environment*, 84:385–392.

Xiao, Z., S. Liang, J. Wang, B. Jiang, and X. Li, 2011. Real-time retrieval of leaf area index from MODIS time series data, *Remote Sensing of Environment*, 115(1):97–106.

Xu, B., P. Gong, and R. Pu, 2003. Crown closure estimation of oak savannah in a dry season with Landsat TM imagery: Comparison of various indices through correlation analysis, *International Journal of Remote Sensing*, 24(9):1811–1822.

Zhang, X., M.A. Friedl, and C.B. Schaaf, 2003. Monitoring vegetation phenology using MODIS, *Remote Sensing of Environment*, 84(3):471–475.

Zhang, X., M.A., Friedl, and C.B. Schaaf, 2006. Global vegetation phenology from Moderate Resolution Imaging Spectroradiometer (MODIS): Evaluation of global patterns and comparison with in situ measurements, *Journal of Geophysical Research*, 111:G04017.

Zheng, G., and L.M. Moskal, 2009. Retrieving Leaf Area Index (LAI) using remote sensing: theories, methods and sensors, *Sensors*, 9(4):2719–2745.